
Disentangling feature and lazy training in deep neural networks

Mario Geiger

Institute of Physics
École Polytechnique Fédérale de Lausanne
CH-1015 Lausanne, Switzerland
mario.geiger@epfl.ch

Stefano Spigler

Institute of Physics
École Polytechnique Fédérale de Lausanne
CH-1015 Lausanne, Switzerland
stefano.spigler@epfl.ch

Arthur Jacot

Institute of Mathematics
École Polytechnique Fédérale de Lausanne
CH-1015 Lausanne, Switzerland
arthur.jacot@epfl.ch

Matthieu Wyart

Institute of Physics
École Polytechnique Fédérale de Lausanne
CH-1015 Lausanne, Switzerland
matthieu.wyart@epfl.ch

Abstract

Two distinct limits for deep learning have been derived as the network width $h \rightarrow \infty$, depending on how the weights of the last layer scale with h . In the Neural Tangent Kernel (NTK) limit, the dynamics becomes linear in the weights and is described by a *frozen* kernel Θ (the NTK). By contrast, in the Mean Field limit, the dynamics can be expressed in terms of the distribution of the parameters associated to a neuron, that follows a partial differential equation. In this work we consider deep networks where the weights in the last layer scale as $\alpha h^{-1/2}$ at initialization. By varying α and h , we probe the crossover between the two limits. We observe two regimes that we call “lazy training” and “feature training”. In the lazy-training regime, the dynamics is almost linear and the NTK does barely change after initialization. The feature-training regime includes the mean-field formulation as a limiting case and is characterized by a kernel that evolves in time, and thus learns some features. We perform numerical experiments on MNIST, Fashion-MNIST, EMNIST and CIFAR10 and consider various architectures. We find that: (i) The two regimes are separated by an α^* that scales as $\frac{1}{\sqrt{h}}$. (ii) Network architecture and data structure play an important role in determining which regime is better: in our tests, fully-connected networks often perform better in the lazy-training regime (except when we reduce the dataset via PCA). However, a convolutional network trained on CIFAR10 with ADAM achieves a lower error in the feature-training regime. (iii) In both regimes, the fluctuations δF induced by initial conditions on the learned function decay as $\delta F \sim 1/\sqrt{h}$, leading to a performance that increases with h . The same improvement can be also obtained at an intermediate width by ensemble-averaging several networks that are trained independently. (iv) In the feature-training regime we identify a time scale $t_1 \sim \sqrt{h}\alpha$, such that for $t \ll t_1$ the dynamics is linear. At $t \sim t_1$, the output has grown by a magnitude \sqrt{h} and the changes of the tangent kernel $\|\Delta\Theta\|$ become significant. Ultimately, it follows $\|\Delta\Theta\| \sim (\sqrt{h}\alpha)^{-a}$ for *ReLU* and *Softplus* activation functions, with $a < 2$ and $a \rightarrow 2$ as depth grows. We provide simple arguments supporting these findings.

1 Introduction and related works

Deep neural networks are successful at a variety of task, yet understanding why they work remains a challenge. A surprising observation is that their performance on supervised tasks keeps increasing with their width h in the over-parametrized regime where they already fit all the training data [Neyshabur et al., 2017, Bansal et al., 2018, Advani and Saxe, 2017, Spigler et al., 2018]. This fact underlines the importance of describing deep learning in the limit $h \rightarrow \infty$, which has received considerable interest recently. When all the weights w of the network are initialized with a value of order $h^{-1/2}$ at initialization, the transmission of the signal through the network in the infinite-width limit is now well understood. The output function $f(w, x)$ at initialization is then a Gaussian random processes with some covariance that can be computed [Neal, 1996, Williams, 1997, Lee et al., 2018, de G. Matthews et al., 2018, Novak et al., 2019, Yang, 2019].

NTK limit More recently, it has been shown that beyond initialization, the learning dynamics in this limit also simplifies [Jacot et al., 2018, Du et al., 2019, Allen-Zhu et al., 2018, Lee et al., 2019, Arora et al., 2019, Park et al., 2019] and is entirely described by the *neural tangent kernel* (NTK) [Jacot et al., 2018] defined as:

$$\Theta(w, x_1, x_2) = \nabla_w f(w, x_1) \cdot \nabla_w f(w, x_2), \quad (1)$$

where x_1, x_2 are two inputs and ∇_w is the gradient with respect to the parameters w . For $h \rightarrow \infty$, $\Theta(w, x_1, x_2) \rightarrow \Theta_\infty(x_1, x_2)$ does not vary at initialization (and thus it does not depend on the specific choice of w) and does not evolve in time. The dynamics is guaranteed to converge on a time independent of h to a global minimum of the loss, and as for usual kernel learning the function only evolves in the space spanned by the functions $\Theta_\infty(x_\mu, x)$, where $\{x_\mu, \mu = 1 \dots n\}$ is the training set.

Mean Field limit Another limit, called mean field in the literature, has been studied in several works focusing mostly on one-hidden layer networks [Mei et al., 2018, Rotskoff and Vanden-Eijnden, 2018, Chizat and Bach, 2018, Sirignano and Spiliopoulos, 2018, Mei et al., 2019, Nguyen, 2019]. In this setting the output function of the network with h hidden neurons corresponding to an input x is

$$f(w, x) = \frac{1}{h} \sum_{i=1}^h c_i \sigma(a_i \cdot x + b_i), \quad (2)$$

where $\sigma(\cdot)$ is the non-linear activation function and $w_i = (a_i, b_i, c_i)$ are the parameters associated with a hidden neuron. Note that the last layer of weights scales as h^{-1} , which differs from the $h^{-1/2}$ scaling used in the NTK setting. At initialization, the terms in the sum are independent random variables. We can invoke the law of large numbers: for large h the average tends to the expectation value

$$f(w, x) \rightarrow \int da db dc \rho(a, b, c) c \sigma(a \cdot x + b), \quad (3)$$

and it has been shown in the literature that the training dynamics is controlled by a differential equation for the density of parameters ρ :

$$\partial_t \rho_t = 2 \nabla \cdot (\rho_t \nabla \Psi(a, b, c; \rho_t)), \quad (4)$$

$$\Psi(a, b, c; \rho) = V(a, b, c) + \int da' db' dc' \rho(a', b', c') U(a, b, c; a', b', c'). \quad (5)$$

Here ∇ is the gradient with respect to (a, b, c) and U, V are potentials defined in [Mei et al., 2018]. This is equivalent to the hydrodynamic (continuous) description of interacting particles in some external potential. The performance of a network is then expected to plateau on approaching this limit, as $h \rightarrow \infty$.

The existence of two distinct limits raises both fundamental and practical questions:

First, which limit best characterizes the neural networks that are used in practice, and which one leads to a better performance? These questions are still debated. In [Chizat and Bach, 2019], based on teacher-student numerical experiments, it was argued that the NTK limit is unlikely to explain the success of neural networks. However, it was recently shown that the NTK limit is able to achieve good performance on real datasets [Arora et al., 2019] (significantly better than alternative kernel methods). Moreover, some predictions of the NTK limit agree with observations in networks of sizes

that are used in practice [Lee et al., 2019].

Second, it was argued that in the NTK limit the surprising improvement of performance with h stems from the $h^{-1/2}$ fluctuations of the kernel at initialization, that ultimately leads to similar fluctuations in the learned function and degrades the performance of networks of small width [Geiger et al., 2019]. These fluctuations can be removed by ensemble-averaging output functions obtained with different initial conditions and trained independently, leading to an excellent performance already near the underparametrized to overparametrized (or *jamming*) transition h^* beyond which all the training data are correctly fitted [Geiger et al., 2018]. Does this line of thought hold true in the mean-field limit?

Finally, unlike in the NTK limit where preactivations vary very weakly during training, in the mean field limit feature training occurs. It is equivalent to saying that the tangent kernel (which can always be defined) evolves in time [Rotskoff and Vanden-Eijnden, 2018, Mei et al., 2019, Chizat and Bach, 2019]. What are the characteristic time scales and magnitude of this evolution?

In this work we answer these questions empirically by learning a model of the form:

$$F(w, x) \equiv \alpha [f(w, x) - f(w_0, x)], \quad (6)$$

where $f(w, x)$ is a deep network. This model is inspired by [Chizat and Bach, 2019]. For $\alpha = \mathcal{O}(1)$ it falls into the framework of the NTK literature, whereas for $\alpha = \mathcal{O}(h^{-1/2})$ it corresponds to the mean-field framework. Our strategy is to consider a specific setup that is fast to train, simple and theoretically tractable. Later, in Section 7, we extend our study to other datasets, architectures including CNNs and dynamics to verify the generality and robustness of our results. We first focus on the Fashion-MNIST dataset for fully-connected (FC) networks with *Softplus* activation functions and gradient-flow dynamics. We study systematically the role of both α (varied on 11 orders of magnitude) and width h , and for each setting learn ensembles of 10 to 20 networks so as to quantify precisely the magnitude of fluctuations induced by initialization, and the benefit of ensemble averaging. Our main result is that in the (α, h) plane two distinct regimes can be identified, in which both performance and dynamics qualitatively differ, although some properties (such as the decay of the fluctuations δF with h) are similar. We provide arguments justifying these findings.

The implications of our work are both practical (in terms of which parameters and architectures lead to improved performance) and conceptual (in quantifying the dynamics of feature training and providing informal explanations for these observations). More generally, it suggests that future empirical studies of deep learning would benefit from characterizing the regime in which they operate, since it will most likely impact their results.

The code used for this article is available online at https://github.com/mariogeiger/feature_lazy.

2 Notations and set-up

The following setup is used for all empirical results in the article, except for those presented in Section 7, where we explore different settings.

We consider deep networks with L hidden layers performing a binary classification task. We denote by w the set of parameters (or weights), and by $f(w, x)$ the output of a network parametrized by w corresponding to an input pattern x . The set of training data is $\mathcal{T} = \{(x_\mu, y_\mu), \mu = 1, \dots, n\}$, where $y_\mu = \pm 1$ is the label associated with the pattern x_μ and n is the number of training data. In what follows \dot{a} is the notation we use for the time derivative of a variable a during training.

Parameter α : Instead of training a network $f(w, x)$, we train $F(w, x) = \alpha(f(w, x) - f(w_0, x))$, i.e we use this quantity as our predictor and train the weights w accordingly. Here w_0 is the network's parameters at initialization. In the over-parametrized regime, this functional form ensures that for $\alpha \rightarrow \infty$, we enter in what we call the lazy-training regime, where changes of weights are small. Indeed in order to obtain a zero loss $\alpha(f(w, x) - f(w_0, x))$ must be $\mathcal{O}(1)$, thus $1 \sim \alpha(f(w, x) - f(w_0, x)) \sim \alpha \nabla_w f(w_0, x) \cdot dw$. For large α then $|f(w, x) - f(w_0, x)|$ is small: the dynamics can hence be considered linear [Chizat and Bach, 2019], with $f(w, x) - f(w_0, x) \approx \nabla_w f(w_0, x) \cdot (w - w_0)$. Since the gradient of $f(w_0, x)$ does not scale with α , this implies that $\|dw\| \equiv \|w - w_0\| \sim \alpha^{-1}$.

Learning is achieved via the minimization of the loss function

$$\mathcal{L}(w) = \frac{1}{\alpha^2 n} \sum_{(x,y) \in \mathcal{T}} \ell(\alpha(f(w, x) - f(w_0, x)), y), \quad (7)$$

where ℓ is the loss per pattern. The prefactor α^{-2} ensures that the convergence time does not depend on α as $\alpha \rightarrow \infty$, since for that choice we have $\alpha \dot{f}(w_0) = \mathcal{O}(1)$.

Note that if we train directly $\alpha f(w, x)$ without removing its value at initialization, we expect no difference with the present setting for α of order one or much smaller. This statement is confirmed numerically in Appendix I. For $\alpha \gg 1$ however, we find empirically that the learning dynamics does not converge.

Dynamics Since our goal is to build a connection between empirical and theoretical approaches, we focus on a discrete version of continuous dynamics obeying simple differential equation. The simplest is the *vanilla gradient descent* which reads $\dot{w} = -\nabla_w \mathcal{L}$ and does not depend on any hyper-parameters. Yet this approach is often too slow. So as to accelerate the dynamics we use *momentum*:

$$\begin{cases} \dot{w} = v, \\ \dot{v} = -\frac{1}{\tau}(v + \nabla_w \mathcal{L}), \end{cases} \quad (8)$$

where v takes the role of a velocity and τ takes the role of a relaxation time. In the $\tau \rightarrow 0$ limit, this dynamics reduces to the vanilla gradient descent. In our experiments we set τ to a fraction of the typical convergence time which happens to scale as $\min(\sqrt{h}\alpha, \sqrt{h}\alpha_c)$, with $\sqrt{h}\alpha_c$ approximately 1 (see Fig. 5 (c)). We tested different values of τ and chose the one that led to faster convergence in terms of computation time while keeping the dynamics close to the vanilla gradient descent; see Appendix G for more details. We took $\tau = 10^{-3} \min(\sqrt{h}\alpha, 10^3)$. This dynamics is run in a discretized form, with a time step that is adapted at each step to ensure that

$$\alpha \max_{x \in \mathcal{T}} |f(w_i, x) - f(w_{i+1}, x)| < 0.1, \quad (9)$$

$$\frac{\|\nabla_w \mathcal{L}_i - \nabla_w \mathcal{L}_{i+1}\|^2}{\|\nabla_w \mathcal{L}_i\| \|\nabla_w \mathcal{L}_{i+1}\|} < \epsilon_{\nabla} = 10^{-4}. \quad (10)$$

In Appendix G we checked that our results are independent of ϵ_{∇} for $\epsilon_{\nabla} \leq 10^{-4}$.

Activation function The *Softplus* activation function is defined as $sp_{\beta}(x) = \frac{1}{\beta} \ln(1 + e^{\beta x})$. The larger the parameter β , the sharper is the *Softplus*, and as $\beta \rightarrow \infty$ it tends to a *ReLU* activation function. In our experiments we take $\beta = 5$. In order to have preactivations of unit variance at initialization we also multiply the *Softplus* by a prefactor $a \approx 1.404$. The activation function that we use at all hidden neurons is then

$$\sigma(x) = a \, sp_{\beta=5}(x) \quad (11)$$

Non-smooth activation functions like ReLU can introduce additional phenomena; for instance, we quantify its impact on the evolution of the neural tangent kernel in Appendix F.

Loss function For the loss-per-pattern $\ell(f, y)$ we use the soft-hinge loss $\ell(f, y) = sp_{\beta}(1 - fy)$, where sp_{β} is again a *Softplus* function. This function is a smoothed version of the hinge loss, to which it tends as $\beta \rightarrow \infty$. We use the value $\beta = 20$ as a compromise between smoothness and being similar to the hinge loss, see Fig. 1. The stopping criterion to end the learning dynamics is met when all patterns are classified within a sufficient margin, that is when $\alpha [f(w, x_{\mu}) - f(w_0, x_{\mu})] y_{\mu} > 1$ for all $\mu = 1, \dots, n$. Keep in mind that this criterion makes sense only in the overparametrized phase (as it will be the case in what follows), where networks manage to fit all the training set [Spigler et al., 2018]. The hinge loss results in essentially identical performance to the commonly used cross-entropy in state-of-the-art architectures, but leads to a dynamics that stops in a finite time in the over-parametrized regime considered here, removing the need to introduce an arbitrary temporal cut-off [Spigler et al., 2018].

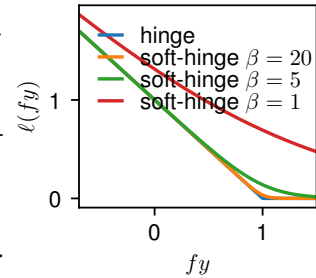


Figure 1: Comparison between the hinge loss and the soft-hinge losses $sp_{\beta}(1 - fy)$ with $\beta = 1, 5, 20$. As β increases, the soft-hinge loss tends to the hinge loss.

Architecture We use a constant-width fully-connected architecture based on [Jacot et al., 2018]. Given an input pattern $x \in \mathbb{R}^d$, we denote by \tilde{z}^ℓ the vector of preactivations at each hidden layer and by z^ℓ the corresponding activations. The flow of signals through the network can be written iteratively as

$$z^\ell = \sigma(\tilde{z}^\ell), \quad (12)$$

$$\tilde{z}^1 = d^{-1/2} W^0 x, \quad (13)$$

$$\tilde{z}^{\ell+1} = h^{-1/2} W^\ell z^\ell, \quad (14)$$

$$f(w, x) = h^{-1/2} W^L z^L. \quad (15)$$

The matrices W^ℓ contain the parameters of the ℓ -th hidden layer, and the (vectorized) set of all these matrices has been previously denoted as w . The width and depth of the network are h and L ; in our simulations we vary h but we mostly keep the depth $L = 3$ constant. The input patterns live a d -dimensional space. Fig. 2 illustrates the architecture and explains our notation. In order to have preactivations of order $\mathcal{O}(1)$ at initialization, all the weights are initialized as standard Gaussian random variables, $W_{ij}^\ell \sim \mathcal{N}(0, 1)$. Note that there is no bias, we discuss it in Appendix J.

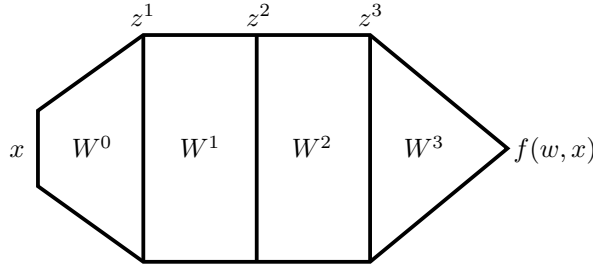


Figure 2: Fully-connected architecture with $L = 3$ hidden layers.

Dataset We train our network to classify 28×28 grayscale images of clothes from the Fashion-MNIST database [Xiao et al., 2017]. For simplicity we split the original 10 classes in two sets and we perform binary classification. For $(x, y) \in \mathcal{T}$ we have $x \in \mathbb{R}^{28 \times 28}$ ($d = 784$) and $y = \pm 1$. The input is normalized on the sphere, $\sum_i x_i^2 = d$ such that each component x_i has unit variance. We took 1000 images of each class (10000 in total) to make our train set and 5000 of each class (50000 in total) to make our test set. The train set is smaller than usual (10000 instead of 50000) in order to shorten the training time.

3 Disentangling feature training and lazy training according to performance

To argue the existence of two distinct regimes in deep neural networks, we evaluate their performance in the (α, h) plane. How we vary parameters to probe this plane is represented in Fig. 3 (a). We consider plots obtained at fixed h and varying α (Fig. 3 (c,d)) as well as fixed $\sqrt{h}\alpha$ (Fig. 3 (b)).

Fig. 3 (b) shows the test error as a function of the width h , for different values of $\sqrt{h}\alpha$. For large h , we observe that as $\sqrt{h}\alpha$ is increased the performance also increases, up to a point where it converges to a limiting curve (for $\sqrt{h}\alpha \geq 10^3$ in the figures). This limiting curve coincides with the test error found if the NTK is frozen at initialization (see Appendix A for a description of our dynamics in that case), represented by a black solid line. We refer to this limiting behavior as lazy training.

There is a value of α for which we leave the lazy-training regime and enter a nonlinear regime that we call feature training. To identify this regime, we show in Fig. 3 (c) the test error as a function of α for several widths h , and the rescaled test error (in such a way that it takes values between 0 and 1) as a function of $\sqrt{h}\alpha$ in Fig. 3 (d). The curves collapse, supporting that in the (α, h) plane the boundary between the two regimes lies at a scale $\alpha^* = \mathcal{O}(h^{-1/2})$. It is precisely the scaling used in Mean Field.

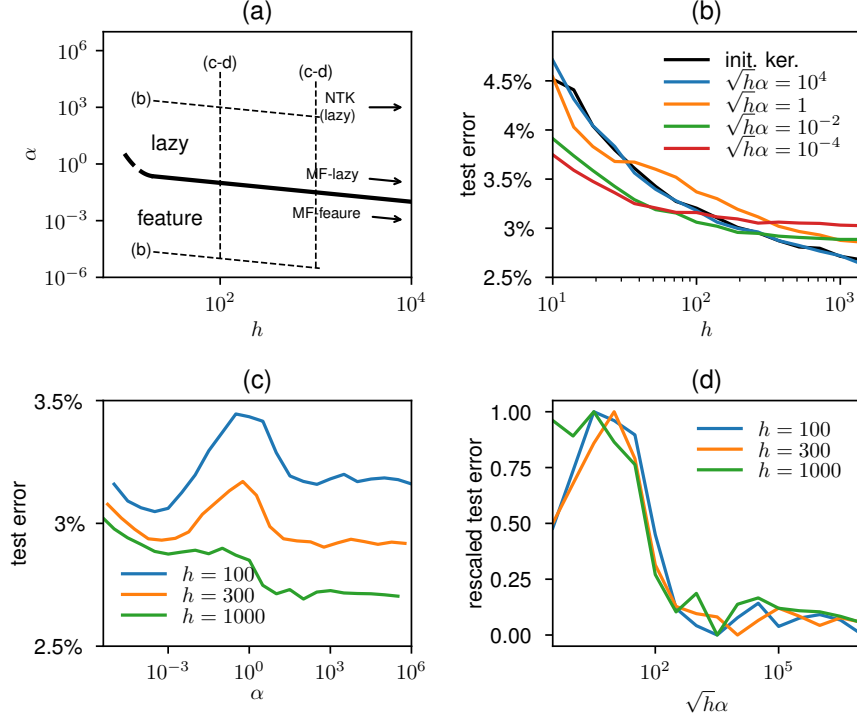


Figure 3: (a) Schematic representation of the parameters that we probe: either we fix $\alpha\sqrt{h}$ or we keep the width h constant and we vary α . The location of the cross-over between the lazy and feature-training regimes is also indicated. (b) Test error v.s. network’s width h for different values of $\sqrt{h\alpha}$ as indicated in legend. The black solid line is the test error of the frozen NTK at initialization, a limit that is recovered as $\alpha\sqrt{h} \rightarrow \infty$. (c) Test error v.s. α , for different widths h . (averaged over 20 initializations) (d) Same data as in (c): after rescaling the test error to be between 0 and 1, the curves collapse when plotted against $\sqrt{h\alpha}$.

4 Fluctuations of the output function and the effect of ensemble averaging

As recalled in Fig. 3, performance increases with h : adding more fitting parameters leads to better predictability and deep networks do not overfit. This surprising behavior was related to the fluctuations of the output function induced by initial conditions, observed to decrease with h [Neal et al., 2019, Geiger et al., 2019]. To quantify the fluctuations in both regimes we train an ensemble of 20 identical functions $F(w_i, x) = \alpha[f(w_i, x) - f(w_{i,0}, x)]$ starting from different initial conditions, and then we measure the ensemble average $\bar{F}(x)$:

$$\bar{F}(x) \equiv \frac{\alpha}{20} \sum_{i=1}^{20} (f(w_i, x) - f(w_{i,0}, x)) \quad (16)$$

A single trained realization of the network fluctuates around the ensemble average $\bar{F}(x)$, and therefore $\delta F(w, x) \equiv F(w, x) - \bar{F}(x)$ is a random function, whose fluctuations are quantified by the variance:

$$\text{Var } F(w, x) = \left\langle [F(w_i, x_\mu) - \bar{F}(x_\mu)]^2 \right\rangle_{\substack{\mu \in \text{test} \\ i \in \text{ensemble}}} \quad (17)$$

where the average is both over the 20 output functions and over all points x_μ in a test set. Other norms can be used to quantify this variance, all yielding the same picture. In Fig. 4 (a-b) we compute these fluctuations either in the feature-training or in the lazy-training regimes. In both cases we find the same decay with the network width:

$$\text{Var } \alpha [f(w, x) - f(w_0, x)] \sim h^{-1}. \quad (18)$$

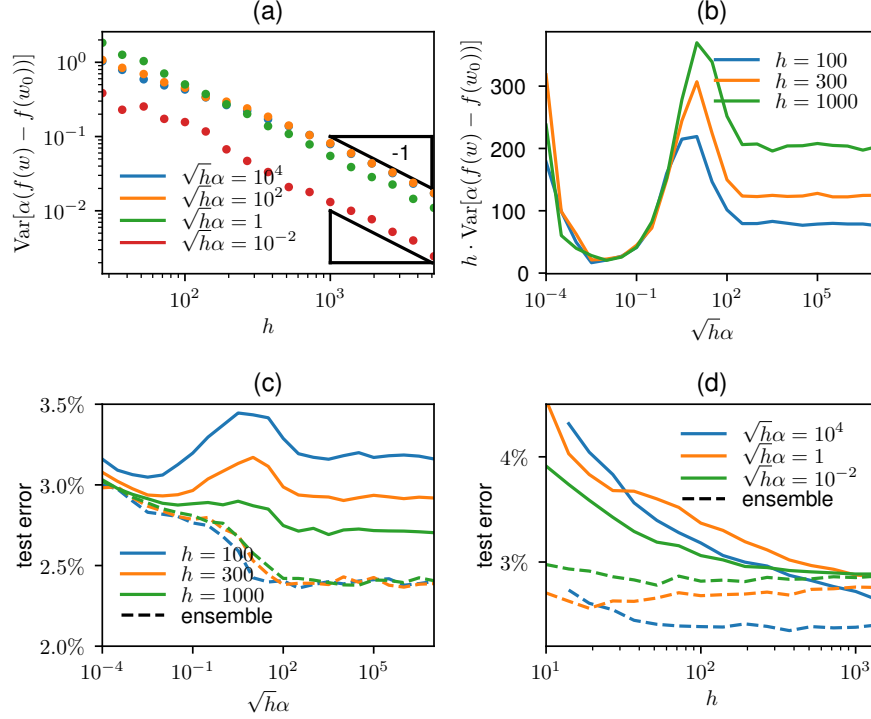


Figure 4: (a) Variance of the network's output v.s. its width h , for different values of $\sqrt{h\alpha}$. In both regimes the variance scales as $\text{Var}[\alpha(f - f_0)] \sim h^{-1}$ (20 initializations per point). For this panel (a) alone, the size of the dataset was reduced to 10^3 because 10^4 requires higher h to observe the asymptotic behavior. See Appendix H for an analysis of the dependence in the size of the dataset. (b) Variance of the network's output times its width v.s. $\sqrt{h\alpha}$, for different network's width. In the lazy-training regime, it needs a larger h (or a smaller n) to observe the overlap of the curves. (c) Test error and ensemble-averaged test error v.s. $\sqrt{h\alpha}$, for several widths h (20 initializations per point). (d) Test error and ensemble-averaged test error v.s. h at fixed values of $\sqrt{h\alpha}$ (20 initializations per point). Once ensemble averaged, lazy training performs better than feature training

Since δF is a random function with zero expectation value and finite variance $\text{Var } F \sim h^{-1}$ we will write that $\delta F \sim h^{-1/2}$.

In Fig. 4 (b), in the lazy-training regime, the curves do not overlap. This is a preasymptotic effect. In Appendix H we show that the asymptotic power law is reached for smaller dataset sizes.

It was argued in [Geiger et al., 2019] that in the lazy-training regime this scaling simply stems from the fluctuations of the NTK at initialization, that go as $\|\delta\Theta\| \sim 1/\sqrt{h}$ and lead to similar fluctuations in δF . These fluctuations were argued to lead to an asymptotic decrease of test error as $1/h$, consistent with observations. Interestingly, the same scaling for the fluctuations holds in the feature-training regime, presumably reflecting the approximations expected from the Central Limit Theorem (CLT) when Eq. (2) is replaced by an integral.

As a consequence of these fluctuations, ensemble averaging output functions leads to an enhanced performance in both regimes, as shown in Fig. 4 (c-d). We remark that:

(i) In each regime, the test error of the ensemble average is essentially independent of h . It implies that the variation of performance with h is only a matter of diminishing fluctuations in the over-parametrized case considered here (as shown below, we always fit all training data in these runs). It also supports that the plateau value of the ensemble-average performance we observe corresponds to the performance of single network in the $h \rightarrow \infty$ limit.

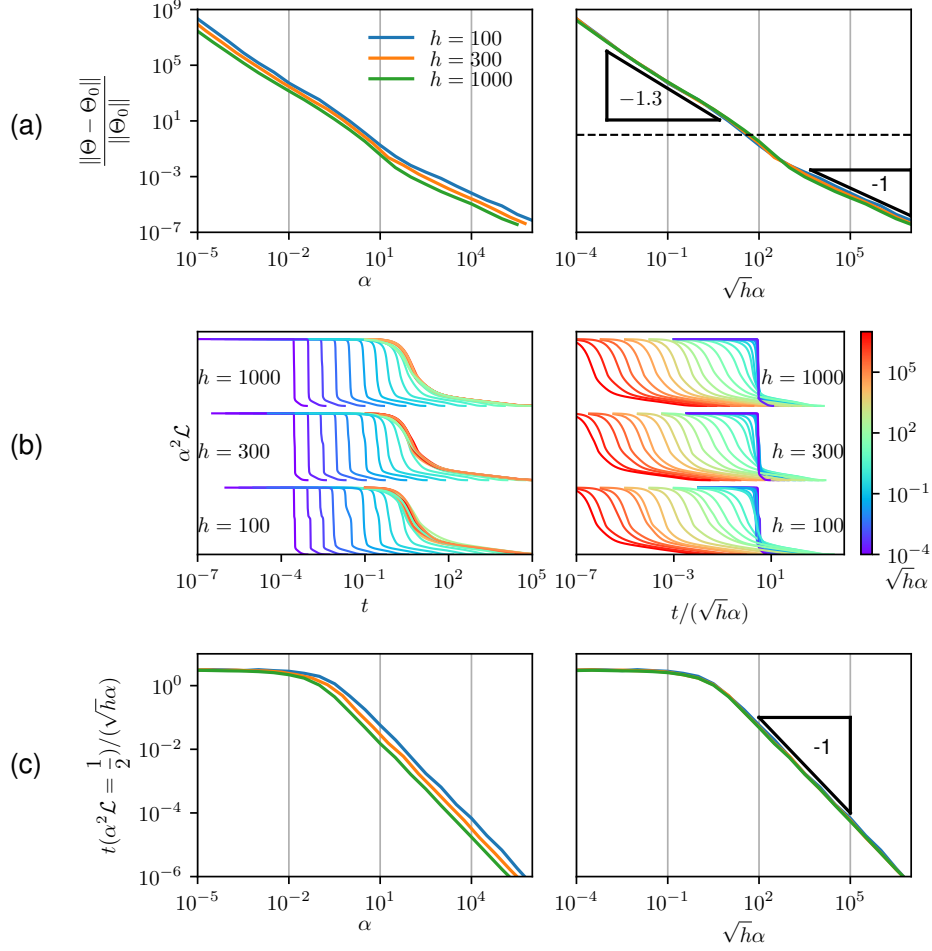


Figure 5: (a) Relative evolution of the kernel $\|\Theta(w) - \Theta(w_0)\| / \|\Theta(w_0)\|$ v.s. α (left) and $\sqrt{h}\alpha$ (right). (b) Rescaled loss $\alpha^2 \mathcal{L}$ v.s. t (left) and $t/\sqrt{h}\alpha$ (right), for three different network’s width and for different values of $\sqrt{h}\alpha$ indicated by the color bar. (c) The time for which the loss is reduced by half v.s. α (left) and $\sqrt{h}\alpha$ (right). (d) t_1, t_2 v.s. α (left) and $\sqrt{h}\alpha$ (right). For (a) and (c) each point is averaged over 10 initializations.

(ii) Interestingly, it is reported in [Geiger et al., 2019] that for a fixed α , the smallest test error of the ensemble average is obtained at some finite h_{\min} beyond h^* implying that past h_{\min} performance is decreasing with growing h . It can now be simply explained: at fixed α one goes from feature to lazy training as h increases, since $\sqrt{h}\alpha$ also increases and must eventually become much larger than one, leading to a change in performance.

(iii) For small values of $\sqrt{h}\alpha$ (smaller than 10^{-4}) the variance blows up. We leave the study of this regime for future works. Since we observe that the test error also greatly increases for these values of $\sqrt{h}\alpha$, this regime is of less interest.

5 Training dynamics differs in the two regimes

The network is able to learn features in the feature-training regime, while it cannot in the lazy-training regime because the NTK is frozen. To quantify feature training we measure the total relative variation of the kernel at the end of training: $\|\Theta(w) - \Theta(w_0)\| / \|\Theta(w_0)\|$, where the norm of a kernel is defined as $\|\Theta(w)\|^2 = \sum_{\mu, \nu \in \text{test set}} \Theta(w, x_\mu, x_\nu)^2$. This quantity is plotted in Fig. 5 (a, left) versus α for

several widths h , and versus $\sqrt{h}\alpha$ in Fig. 5 (a, right). The fact that the curves collapse indicates that $\alpha\sqrt{h}$ is the parameter that controls feature training. In particular, the crossover $\alpha^* \sim h^{-1/2}$ precisely corresponds to the point where the change of the kernel is of the order of the norm of the kernel at initialization. Moreover, in the feature-training regime we find:

$$\|\Theta(w) - \Theta(w_0)\|/\|\Theta(w_0)\| \sim (\sqrt{h}\alpha)^{-a}, \quad (19)$$

with an exponent $a \approx 1.3$. By contrast in the lazy-training regime $\|\Theta(w) - \Theta(w_0)\|/\|\Theta(w_0)\| \sim 1/(\sqrt{h}\alpha)$, as expected for what concerns the dependency in h [Jacot et al., 2019, Geiger et al., 2019, Lee et al., 2019].

In Appendix C, we show in Fig. 8 an example of the evolution of the kernel (represented by its Gram matrix). We also present an interesting discovery: once the network has been trained, performing kernel learning with the NTK obtained at the end essentially leads to the same generalization error.

We finally investigate the temporal evolution of learning, known to be characterized by several time scales [Baity-Jesi et al., 2018]. The rescaled loss $\alpha^2 \mathcal{L}$ is shown in Fig. 5 (b). As expected [Jacot et al., 2018, Chizat and Bach, 2019], in the lazy-training regime $\mathcal{L}(t)$ depends neither on α nor h . This is not true in feature training however. We define t_1 as the time point where the loss decreases by 50%. Our key finding, shown in Fig. 5 (c), is that in the feature-training regime:

$$t_1 \sim \alpha\sqrt{h}. \quad (20)$$

In Appendix C we show that, in the feature-training regime, t_1 also marks the timescale below which the dynamics remains linear.

6 Arguments on kernel dynamics and regimes' boundary

The arguments proposed in this section do not have the status of mathematical proofs. They provide heuristic explanations for the scaling $t_1 \sim \alpha\sqrt{h}$ and $\alpha^* \sim 1/\sqrt{h}$, and support that the output function grows by a factor \sqrt{h} before the dynamics become highly non-linear. A simple assumption on the nature of the ensuing non-linear dynamics leads to the prediction Eq. (19) with $a = 2/(1 + 1/L)$, which we view as a good approximation (not necessarily exact) of our observations.

Our starting point is that for the NTK initialization, we have at $t = 0$ that $\tilde{z}_\alpha = \mathcal{O}(1)$ and $\partial f/\partial \tilde{z}_\alpha = \mathcal{O}(1/\sqrt{h})$, where \tilde{z}_α is the preactivation of a hidden neuron. The second point can be derived iteratively starting from the last hidden layer. Denote by W^0 the weight matrix connected to the input, and W^ℓ the weight matrix connecting two hidden neurons in the $\ell - 1$ and ℓ hidden layers respectively, and W^L the weight vector connected to the output. It is then straightforward to show using the chain rule and $\sigma'(\tilde{z}) = \mathcal{O}(1)$ that (see also [Arora et al., 2019]):

$$\frac{\partial f}{\partial W^0} = \mathcal{O}\left(\frac{1}{\sqrt{h}}\right); \quad \frac{\partial f}{\partial W^\ell} = \mathcal{O}\left(\frac{1}{h}\right); \quad \frac{\partial f}{\partial W^L} = \mathcal{O}\left(\frac{1}{\sqrt{h}}\right). \quad (21)$$

From which we deduce that:

$$\dot{W}^0 = \mathcal{O}\left(\frac{1}{\sqrt{h}\alpha}\right); \quad \dot{W}^\ell = \mathcal{O}\left(\frac{1}{h\alpha}\right); \quad \dot{W}^L = \mathcal{O}\left(\frac{1}{\sqrt{h}\alpha}\right) \quad (22)$$

by applying gradient descent.

Next, we consider how the neurons' preactivations evolve in time. From the composition of derivatives, one obtains $\dot{\tilde{z}}^{\ell+1} = h^{-1/2}(\dot{W}^\ell z^\ell + W^\ell \dot{z}^\ell)$. It is clear from Eq. (22) that $h^{-1/2}\dot{W}^\ell z^\ell = \mathcal{O}\left(\frac{1}{\sqrt{h}\alpha}\right)$.

Concerning the product $W^\ell \dot{z}^\ell$, in the large-width limit it can be proven to be correctly estimated by considering that W^ℓ and \dot{z}^ℓ are independent [Dyer and Gur-Ari, 2019]. (This result simply stems from the fact that the time-derivative of the preactivation of one neuron depends on all its h outgoing weights, and is therefore weakly correlated to any of them). From the central limit theorem, the vector $W^\ell \dot{z}^\ell$ is thus of order $\sqrt{h}\dot{z}^\ell$. Proceeding recursively from the input to the output we obtain:

$$\dot{\tilde{z}}^\ell = \mathcal{O}\left(\frac{1}{\sqrt{h}\alpha}\right). \quad (23)$$

We checked Eq. (23) numerically in Appendix D.

From Eq. (22) and Eq. (23) we expect that:

$$\forall t \ll t_1 \equiv \alpha\sqrt{h}, \quad W^L(t) - W^L(0) = o(1); \quad \tilde{z}^\ell(t) - \tilde{z}^\ell(0) = o(1) \quad (24)$$

Thus for $t \ll t_1$, we are in the lazy-training regime where preactivations and weights did not have time to evolve, and we expect the kernel variations to be small (see [Mei et al., 2019] for a related discussion). Since the lazy-training regime finds a zero loss solution and stops in a time $\mathcal{O}(1)$ (see Section 2), if $t_1 = \alpha\sqrt{h} \gg 1$ the network remains in it throughout learning. Thus $\alpha^* \sim 1/\sqrt{h}$, as proposed for a single layer in [Chizat and Bach, 2019].

By contrast, if $\alpha\sqrt{h} \ll 1$ the dynamics has not stopped at times $t \sim t_1$, for which we have $W^L(t_1) - W^L(0) = \mathcal{O}(1)$ and $\tilde{z}(t_1) - \tilde{z}(0) = \mathcal{O}(1)$: both the preactivations and the weights of the last layer have changed significantly, leading to significant changes of $\nabla_w f$ and Θ . It is important to note that at $t \sim t_1$, the scale of the output function is expected to change. Indeed at initialization the output function, which is a sum made on the last layer of hidden neurons $f(w, x) = \frac{1}{\sqrt{h}} \sum_{i=1}^h W_i^L \sigma(\tilde{z}_i^L)$, is $\mathcal{O}(1)$ as expected from the CLT applied to h uncorrelated terms [Neal, 1996]. However, for $t \sim t_1$ this independence does not hold anymore, since the terms $W_i^L \sigma(\tilde{z}_i^L)$ have evolved by $\mathcal{O}(1)$ to change the function $f(w, x)$ in a specific direction. We thus expect these correlations to build up linearly in time for $t \in [0, t_1]$ and to ultimately increase the output by a factor \sqrt{h} at $t \sim t_1$, as confirmed in Appendix C. Note that this effect does not appear at intermediate layers in the network, because the weights evolve much more slowly there as follows from Eq. (22).

Still, such an increase in the output is insufficient to find solutions deep in the feature-training regime, since $\alpha[f(w(t_1)) - f(w(0))] \sim \alpha\sqrt{h} \ll 1$. We propose that for activation functions that increase linearly at large arguments as those we use, the dynamics for $t \approx t_1$ approximately corresponds to an inflation of the weights along the direction $\dot{w}(t_1)$. Specifically, we define an amplification factor $\lambda(t) = \|w(t) - w(0)\|/\|w(t_1) - w(0)\|$, and assume for simplicity that this amplification is identical in each of the $L + 1$ layers of weights (we disregard in particular the fact that the last and first layer may behave differently, as discussed in [Arora et al., 2019]). By definition, $\lambda(t_1) = 1$. At the end t_2 of training, for activation functions that increase linearly at large arguments, we expect to have $\lambda(t_2) \sim [\alpha\sqrt{h}]^{-1/(L+1)}$ to ensure that $\alpha[f(w(t_2)) - f(w(0))] = \mathcal{O}(1)$. Gradient with respect to weights are increased by λ^L , leading to an overall inflation of the kernel:

$$\Theta(t_2) - \Theta(0) \sim \Theta(t_2) \sim \lambda^{2L} \sim [\alpha\sqrt{h}]^{-\frac{2}{1+1/L}} \quad (25)$$

leading to $a = 1.66$ consistent with Eq. (19). We have checked this prediction with success for shallow networks with $L = 2$, as shown in Appendix E.

7 Other experiments

We now check that our conclusions extend to other data sets, architectures and learning dynamics. In particular we consider under which circumstances feature training outperforms lazy training. Table 1 summarizes our results. The key observation is that which regime works best depends on the architecture and on the data. In particular, for the training set size 10^4 we focus on in this study (as it allows to study gradient descent in a reasonable time), we generally find that FCC performs better

Table 1: Performance for different setups.

Architecture	Dataset (binary, 10k)	Algorithm	Regime performing better
CNN (4 hidden layers)	CIFAR10	ADAM (batch size 32)	feature training
CNN (4 hidden layers)	Fashion-MNIST	ADAM (batch size 32)	Not clear (Fig. 7(b))
FC (3 hidden layers)	CIFAR10	ADAM (batch size 32)	lazy training
FC (3,9 hidden layers)	Fashion-MNIST	Gradient flow	lazy training
FC (3 hidden layers)	MNIST	Gradient flow	lazy training
FC (3 hidden layers)	EMNIST letters	Gradient flow	lazy training
FC (3 hidden layers)	CIFAR10	Gradient flow	lazy training
FC (5 hidden layers)	MNIST 10 PCA	Gradient flow	feature training

under the lazy training regime. For the CNN architectures we study lazy training tends to perform better.

MNIST and CIFAR10: We train the FC network defined in Section 2 on the MNIST and CIFAR10 datasets. In Fig. 6 we show the results. The picture is qualitatively similar to what we see for Fashion-MNIST.

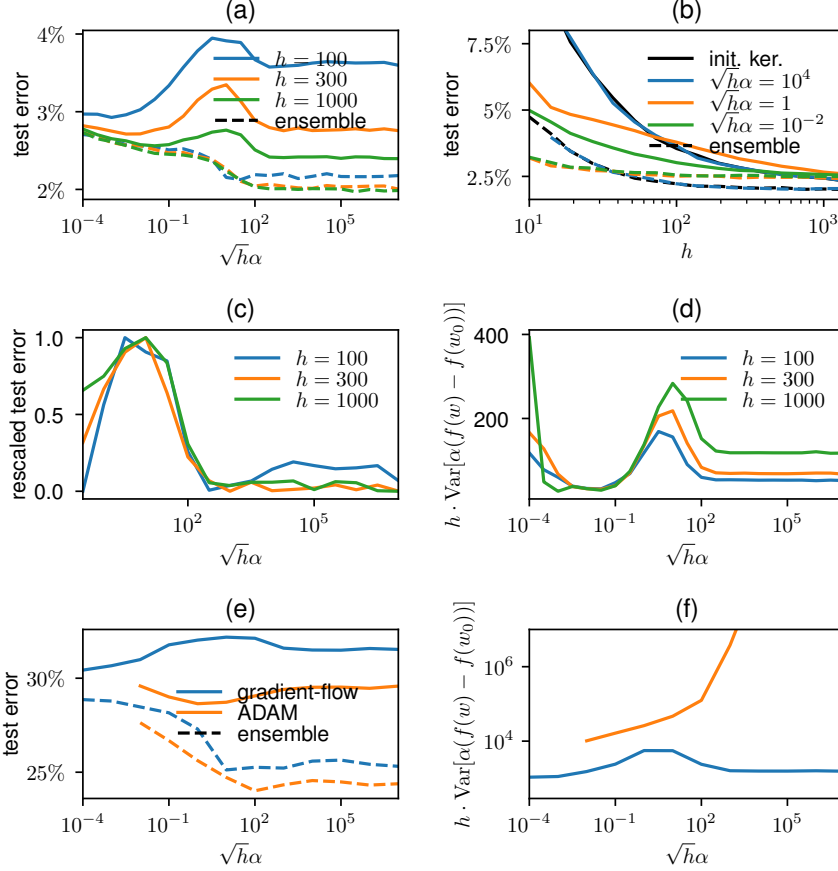


Figure 6: Binary classification on MNIST (a-d) and CIFAR10 (e-f) with the setup presented in Section 2. (a) MNIST test error (single shot and ensemble average over 20 instances) v.s. $\sqrt{h\alpha}$ for different widths h . (b) MNIST test error v.s. the width h for different values of $\sqrt{h\alpha}$. The black lines is the test error of the frozen NTK at initialization, limit that is recovered as $\alpha \rightarrow \infty$. Ensemble averages are computed over 10 instances. (c) Same data as in (a): after rescaling the test error to be in $(0, 1)$ the curves collapse when plotted against $\sqrt{h\alpha}$. (d) The network's width times the variance of the output v.s. $\sqrt{h\alpha}$ for different widths h . This plot is computed for the MNIST dataset and is averaged over 20 initializations. (e) CIFAR10 test error (single shot and ensemble average over 20 instances) v.s. $\sqrt{h\alpha}$ for a network of width $h = 100$. (f) The network's width times the variance of the output v.s. $\sqrt{h\alpha}$. This plot is computed for the CIFAR10 dataset and is averaged over 20 initializations.

First ten principal components of MNIST PCA: As dataset we consider the projection of the handwritten digits in the MNIST dataset onto their first 10 principal components, obtained via principal-component analysis (PCA). This dataset is harder to fit than the original MNIST. Using the FC network defined in Section 2, we observe (see Fig. 7 (a)) that the test error for a single network as well as the ensemble-averaged test error are nearly identical, even somewhat smaller in

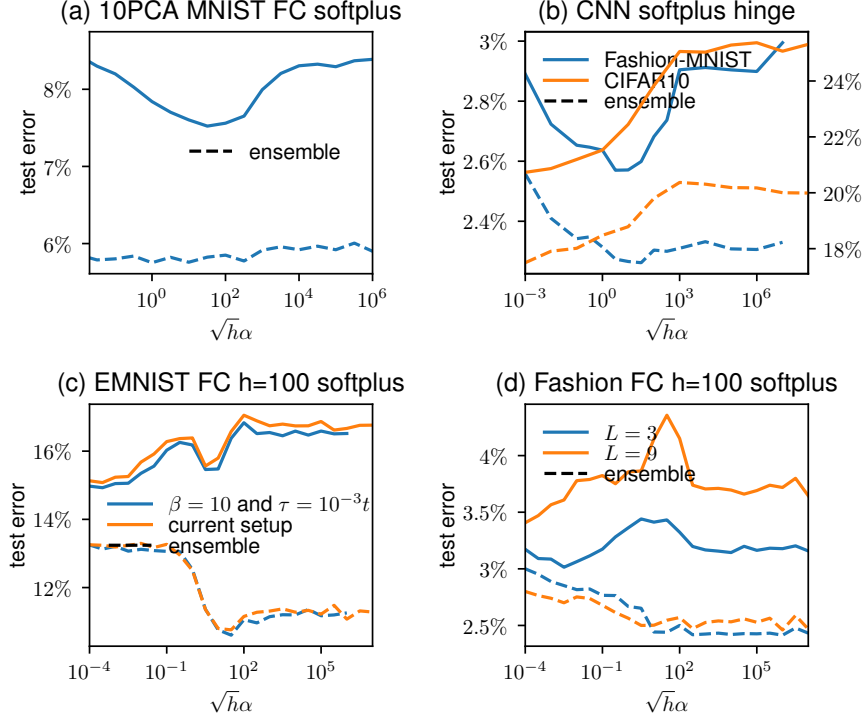


Figure 7: Test error and ensemble average test error v.s. $\sqrt{h}\alpha$ for different setup. (a) MNIST reduced to its first 10 PCA component trained on FC of width 100. (b) CIFAR10 trained on a CNN with the hinge loss and ADAM. (c) The letters from EMNIST. (d) Two different depth on Fashion-MNIST.

the feature-learning regime than in the lazy-learning regime, contrarily to what was observed for the full MNIST dataset.

EMNIST: Using again the FC network defined in Section 2, we consider the pictures of handwritten letters in the EMNIST dataset. Fig. 7 (c) shows that the results are similar to what observed for Fashion-MNIST and MNIST. Here two setups are compared, the current setup (described in Section 2) and an alternative setup with $\beta = 10$ for the loss function and a value of τ proportional to the time.

CNN for CIFAR 10 and Fashion-MNIST: We train a convolutional neural network (CNN) with 4 hidden layers (with stride and padding). It has *Softplus* activation function and no biases. We initialize the parameters of the convolutional networks as standard Gaussians in such a way that the preactivations are of order unity. Our architecture has 4 hidden layers, and we use a stride of $/2$ before the first layer and in the middle of the network. After the convolutions we average the spatial dimensions, and the last layer is a simple perceptron. The code is available on the repository. It is trained to classify images of the CIFAR10 dataset. Learning is achieved with the ADAM dynamics [Kingma and Ba, 2015]. We observe, see Fig. 7 (b), that individual and ensemble-averaged performance is better in the feature-learning regime. For Fashion-MNIST, the optimal performance occurs in a narrow range of intermediate α .

Effect of Depth: In Fig. 7 (d) we compare networks with different depths, $L = 3$ with $L = 9$. The setup is defined in Section 2. We find that increasing depth does not change qualitatively the dependence of the test error with $\sqrt{h}\alpha$. Quantitatively, depth has a very limited effect on the ensemble average performance, but does decrease the performance of individual networks — presumably indicating that depth increases fluctuations of the output function induced by random initialization.

8 Conclusion

We have shown that as the width h and the output scale α at initialization are varied, two regimes appear depending on the value of $\alpha\sqrt{h}$. In the feature-training regime features are learned (in the sense that the tangent kernel evolves during training), whereas in the lazy-learning regime the dynamics is controlled by a frozen kernel. Our key findings are that: (i) In both regimes, fluctuations induced by initialization decrease with h , explaining why performance increases with the width. (ii) In feature training, the learning dynamics is linear for $t \ll t_1 \sim \sqrt{h}\alpha$, time at which the output of the model becomes of order $\sqrt{h}\alpha$. If $\sqrt{h}\alpha \ll 1$, in order to fit the data the dynamics enters a non-linear regime for $t \sim t_1$ that affects the magnitude of the kernel.

On the empirical side, our work supports that studies of deep learning (e.g. on the role of regularization) should specify in which regime their networks operate, since it is very likely that it affects their results. On the theoretical side, there is little quantitative understanding on how much the performance should differ in two regimes. The results that we presented in Section 7 show that it depends on both the structure of the data and on the architecture of the network. Answering this point appears necessary to ultimately understand why deep learning works.

Acknowledgements

We thank Levent Sagun, Clément Hongler, Franck Gabriel, Giulio Biroli, Stéphane d’Ascoli for helpful discussions. We thank Riccardo Rivasio and Jonas Paccolat for proofreading. This work was partially supported by the grant from the Simons Foundation (#454953 Matthieu Wyart). M.W. thanks the Swiss National Science Foundation for support under Grant No. 200021-165509.

References

- M. S. Advani and A. M. Saxe. High-dimensional dynamics of generalization error in neural networks. *arXiv preprint arXiv:1710.03667*, 2017.
- Z. Allen-Zhu, Y. Li, and Z. Song. A convergence theory for deep learning via over-parameterization. *arXiv preprint arXiv:1811.03962*, 2018.
- S. Arora, S. S. Du, W. Hu, Z. Li, R. Salakhutdinov, and R. Wang. On exact computation with an infinitely wide neural net. *arXiv preprint arXiv:1904.11955*, 2019.
- M. Baity-Jesi, L. Sagun, M. Geiger, S. Spigler, G. B. Arous, C. Cammarota, Y. LeCun, M. Wyart, and G. Biroli. Comparing dynamics: Deep neural networks versus glassy systems. In J. Dy and A. Krause, editors, *Proceedings of the 35th International Conference on Machine Learning*, volume 80 of *Proceedings of Machine Learning Research*, pages 314–323, Stockholmsmässan, Stockholm Sweden, 10–15 Jul 2018. PMLR. URL <http://proceedings.mlr.press/v80/baity-jesi18a.html>.
- Y. Bansal, M. Advani, D. D. Cox, and A. M. Saxe. Minnorm training: an algorithm for training overcomplete deep neural networks. *arXiv preprint arXiv:1806.00730*, 2018.
- L. Chizat and F. Bach. On the Global Convergence of Gradient Descent for Over-parameterized Models using Optimal Transport. In *Advances in Neural Information Processing Systems 31*, pages 3040–3050. Curran Associates, Inc., 2018.
- L. Chizat and F. Bach. A Note on Lazy Training in Supervised Differentiable Programming. working paper or preprint, Feb. 2019. URL <https://hal.inria.fr/hal-01945578>.
- A. G. de G. Matthews, J. Hron, M. Rowland, R. E. Turner, and Z. Ghahramani. Gaussian process behaviour in wide deep neural networks. In *International Conference on Learning Representations*, 2018. URL <https://openreview.net/forum?id=H1-nGgWC->.
- S. S. Du, X. Zhai, B. Póczos, and A. Singh. Gradient descent provably optimizes over-parameterized neural networks. In *International Conference on Learning Representations*, 2019. URL <https://openreview.net/forum?id=S1eK3i09YQ>.

- E. Dyer and G. Gur-Ari. Asymptotics of wide networks from feynman diagrams. *arXiv preprint arXiv:1909.11304*, 2019.
- M. Geiger, S. Spigler, S. d’Ascoli, L. Sagun, M. Baity-Jesi, G. Biroli, and M. Wyart. The jamming transition as a paradigm to understand the loss landscape of deep neural networks. *arXiv preprint arXiv:1809.09349*, 2018.
- M. Geiger, A. Jacot, S. Spigler, F. Gabriel, L. Sagun, S. d’Ascoli, G. Biroli, C. Hongler, and M. Wyart. Scaling description of generalization with number of parameters in deep learning. *arXiv preprint arXiv:1901.01608*, 2019.
- A. Jacot, F. Gabriel, and C. Hongler. Neural tangent kernel: Convergence and generalization in neural networks. In *Proceedings of the 32Nd International Conference on Neural Information Processing Systems, NIPS’18*, pages 8580–8589, USA, 2018. Curran Associates Inc. URL <http://dl.acm.org/citation.cfm?id=3327757.3327948>.
- A. Jacot, F. Gabriel, and C. Hongler. The asymptotic spectrum of the hessian of dnn throughout training. *arXiv preprint arXiv:1910.02875*, 2019.
- D. P. Kingma and J. Ba. Adam: A method for stochastic optimization. *International Conference on Learning Representations*, 2015.
- J. Lee, L. Xiao, S. S. Schoenholz, Y. Bahri, J. Sohl-Dickstein, and J. Pennington. Wide neural networks of any depth evolve as linear models under gradient descent. *arXiv preprint arXiv:1902.06720*, 2019.
- J. H. Lee, Y. Bahri, R. Novak, S. S. Schoenholz, J. Pennington, and J. Sohl-Dickstein. Deep neural networks as gaussian processes. *ICLR*, 2018.
- S. Mei, A. Montanari, and P.-M. Nguyen. A mean field view of the landscape of two-layers neural networks. *arXiv preprint arXiv:1804.06561*, 2018.
- S. Mei, T. Misiakiewicz, and A. Montanari. Mean-field theory of two-layers neural networks: dimension-free bounds and kernel limit. *arXiv preprint arXiv:1902.06015*, 2019.
- B. Neal, S. Mittal, A. Baratin, V. Tantia, M. Scicluna, S. Lacoste-Julien, and I. Mitliagkas. A modern take on the bias-variance tradeoff in neural networks. 2019. URL <https://openreview.net/forum?id=HkgmzhC5F7>.
- R. M. Neal. *Bayesian Learning for Neural Networks*. Springer-Verlag New York, Inc., Secaucus, NJ, USA, 1996. ISBN 0387947248.
- B. Neyshabur, R. Tomioka, R. Salakhutdinov, and N. Srebro. Geometry of optimization and implicit regularization in deep learning. *arXiv preprint arXiv:1705.03071*, 2017.
- P.-M. Nguyen. Mean field limit of the learning dynamics of multilayer neural networks. *arXiv preprint arXiv:1902.02880*, 2019.
- R. Novak, L. Xiao, Y. Bahri, J. Lee, G. Yang, D. A. Abolafia, J. Pennington, and J. Sohl-dickstein. Bayesian deep convolutional networks with many channels are gaussian processes. In *International Conference on Learning Representations*, 2019. URL <https://openreview.net/forum?id=Big30j0qF7>.
- D. S. Park, J. Sohl-Dickstein, Q. V. Le, and S. L. Smith. The effect of network width on stochastic gradient descent and generalization: an empirical study. *arXiv preprint arXiv:1905.03776*, 2019.
- G. M. Rotskoff and E. Vanden-Eijnden. Neural networks as interacting particle systems: Asymptotic convexity of the loss landscape and universal scaling of the approximation error. *arXiv preprint arXiv:1805.00915*, 2018.
- J. Sirignano and K. Spiliopoulos. Mean field analysis of neural networks. *arXiv preprint arXiv:1805.01053*, 2018.

- S. Spigler, M. Geiger, S. d’Ascoli, L. Sagun, G. Biroli, and M. Wyart. A jamming transition from under-to over-parametrization affects loss landscape and generalization. *arXiv preprint arXiv:1810.09665*, 2018.
- C. K. Williams. Computing with infinite networks. In *Advances in neural information processing systems*, pages 295–301, 1997.
- H. Xiao, K. Rasul, and R. Vollgraf. Fashion-mnist: a novel image dataset for benchmarking machine learning algorithms, 2017.
- G. Yang. Scaling limits of wide neural networks with weight sharing: Gaussian process behavior, gradient independence, and neural tangent kernel derivation. *arXiv preprint arXiv:1902.04760*, 2019.
- S. Zagoruyko and N. Komodakis. Wide residual networks. In *BMVC*, 2016.

A Frozen NTK dynamics

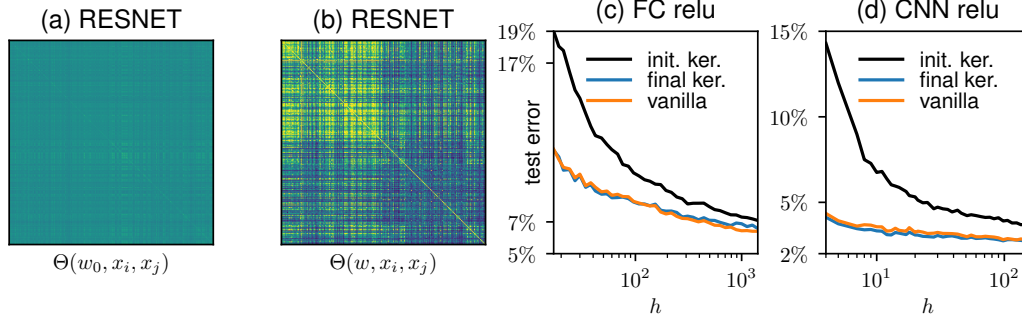


Figure 8: Gram matrix of the test set at initialization $\Theta(w_0, x_\mu, x_\nu)$ (a) and at the end of training $\Theta(w, x_\mu, x_\nu)$ (b), for a wide-resnet 28x10 architecture [Zagoruyko and Komodakis, 2016] ($L = 25$ hidden layers) trained on a binary version of CIFAR10. The first half of the indices $\mu = 1 \dots n/2$ has label $y = 1$ and the other half has label $y = -1$. The kernel inflates during learning in a way that depends on the two classes. See Appendix A for a description of the architecture. (c-d) Test error v.s. the width h for the regular dynamics, the dynamics with the frozen kernel at initialization and the dynamics with the frozen kernel of the end of training. The training performance is captured by the kernel.

Let us consider the first order approximation $\tilde{f}_{w_1}(w, x)$ of a model $f(w, x)$ around $w = w_1$,

$$\tilde{f}_{w_1}(w, x) = \nabla_w f(w_1, x) \cdot w. \quad (26)$$

For instance, w_1 can be the value at initialization or at the end of another dynamics. We can then train this linearized model keeping the gradients fixed:

$$\dot{\tilde{f}}_{w_1}(w) = \nabla_w f(w_1) \cdot \dot{w}, \quad (27)$$

where \dot{w} depends on the gradient descent procedure. Using gradient descent with momentum as in Eq. (8),

$$\begin{aligned} \dot{\tilde{f}}_{w_1}(w) &= \nabla_w f(w_1) \cdot v, \\ -\tau \dot{v} &= v + \frac{1}{n} \sum_{(x,y) \in \mathcal{T}} \ell'(\tilde{f}_{w_1}(w, x), y) \nabla_w f(w_1, x). \end{aligned} \quad (28)$$

If we define $\tilde{v} = \nabla_w f(w_1) \cdot v$ we can rewrite the previous equation as

$$\begin{aligned} \dot{\tilde{f}}_{w_1}(w) &= \tilde{v} \\ -\tau \dot{\tilde{v}} &= \tilde{v} + \frac{1}{n} \sum_{(x,y) \in \mathcal{T}} \ell'(\tilde{f}_{w_1}(w, x), y) \Theta(w_1, x), \end{aligned} \quad (29)$$

where Θ is the neural tangent kernel defined in Eq. (1). We call these equations the *frozen kernel dynamics*.

The results presented in Fig. 5 state that the network learns a kernel during the training dynamics, and that this learned kernel coincides with the frozen kernel in the lazy-training regime as $\sqrt{h}\alpha \rightarrow \infty$. Another way to see that the kernel changes during training is to plot the so-called Gram matrix of the frozen kernel, namely the matrix $(\Theta(w, x_\mu, x_\nu))_{\mu, \nu \in \text{test set}}$: in Fig. 8 (a-b) we show the Gram matrix of the neural tangent kernel evaluated before and after training, where it is clear that there is an emergent structure that depends on the dataset.

The architecture used in in Fig. 5 is a resnet based on [Zagoruyko and Komodakis, 2016]. We use no batch normalization and initialization is as in our fully-connected networks. The code describing the architecture is available in the supplementary material.

It is interesting to test if the performance of deep networks after learning is entirely encapsulated in the kernel it has learned. We argue that indeed this is the case, and to make our point, we proceed as follows. At any time t during training, we can compute the instantaneous neural tangent kernel $\Theta(w(t))$ as in Eq. (1); then, we perform a frozen kernel dynamics using that instantaneous kernel,

and we evaluate its performance on the test set. In Fig. 8 (c-d) we plot the test error of a network with $\alpha = 1$ (referred to as “vanilla”) and compare it to the test error of the frozen kernel, both at initialization ($t = 0$) and at the end of training. Quite remarkably $\tilde{f}_{w(t_2)}$ achieves the full performance of f .

B Dynamics of the Weights

In Fig. 9 we plot the rescaled evolution of the parameters $\sqrt{h}\|w - w_0\|/\|w_0\|$ versus α (left) and versus $\sqrt{h}\alpha$ (right) showing that the curves collapse. We find:

$$\frac{\|w - w_0\|}{\|w_0\|} \sim \frac{1}{h\alpha} \quad (30)$$

in the lazy-training regime. It is expected from Eq. (22), and the fact that the dynamics lasts $\mathcal{O}(1)$ in this regime, jointly implying that the $\mathcal{O}(h^2)$ internal weights evolve by $\mathcal{O}(1/(h\alpha))$. Finally

$$\frac{\|w - w_0\|}{\|w_0\|} \sim \frac{(\sqrt{h}\alpha)^{-b}}{\sqrt{h}} \quad (31)$$

in the feature-training regime, where $b \approx 0.23$ is compatible with $1/(L+1) \approx 0.17$ as proposed in Section 6. Note that the denominator \sqrt{h} is also expected from Section 6, where it corresponds to the term $\|w(t_1) - w(0)\|$ entering in the definition of λ . It comes from the fact that $\|w(t_1) - w(0)\| \sim \sqrt{h}$, as follows from the $\mathcal{O}(h^2)$ internal weights evolving by $\mathcal{O}(1/\sqrt{h})$ on the time scale t_1 , as can be deduced from Eq. (22).

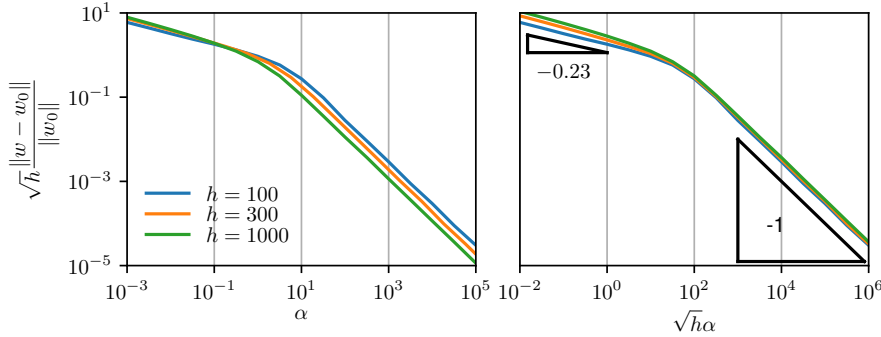


Figure 9: Relative evolution of the parameters $\sqrt{h}\|w - w_0\|/\|w_0\|$ v.s. α (left) and $\sqrt{h}\alpha$ (right). Each measure is averaged over 10 initializations.

C Dynamics of the Output function

To measure the amplitude of the output of a network f we define its norm as follow

$$\|f(w)\| = \sqrt{\langle f(w, x_\mu)^2 \rangle_{\mu \in \text{test}}} \quad (32)$$

In Section 6 we argued that the dynamics is linear for $t \ll t_1 \sim \alpha\sqrt{h}$. Fig. 10 (a,c,d) confirms that the dynamics, characterized by $\|f(w_t) - f(w_0)\|$, is indeed linear on a time scale of order t_1 , independently of the value of α as shown in Fig. 10 (a) or h as shown in Fig. 10 (c,d).

Another important result of Section 6 is that at the end of the linear regime, the output has increased by a relative amount $\sim \sqrt{h}$. This result is confirmed in Fig. 10(b) showing that $\frac{1}{\sqrt{h}}\|f(w_t)\|$ is independent of h for $t \sim t_1$.

These two facts taken together imply:

$$\|f(w_t) - f(w_0)\| \sim \frac{t}{t_1} \sqrt{h}, \quad t \ll t_1 \text{ in feature training.} \quad (33)$$

This prediction is confirmed in Fig. 10 (d) showing $\alpha \|f(w_t) - f(w_0)\| \sim t/t_1 (\sqrt{h}\alpha)$ which must behave as t/t_1 if $(\sqrt{h}\alpha)$ is hold fixed, as is the case in this figure.

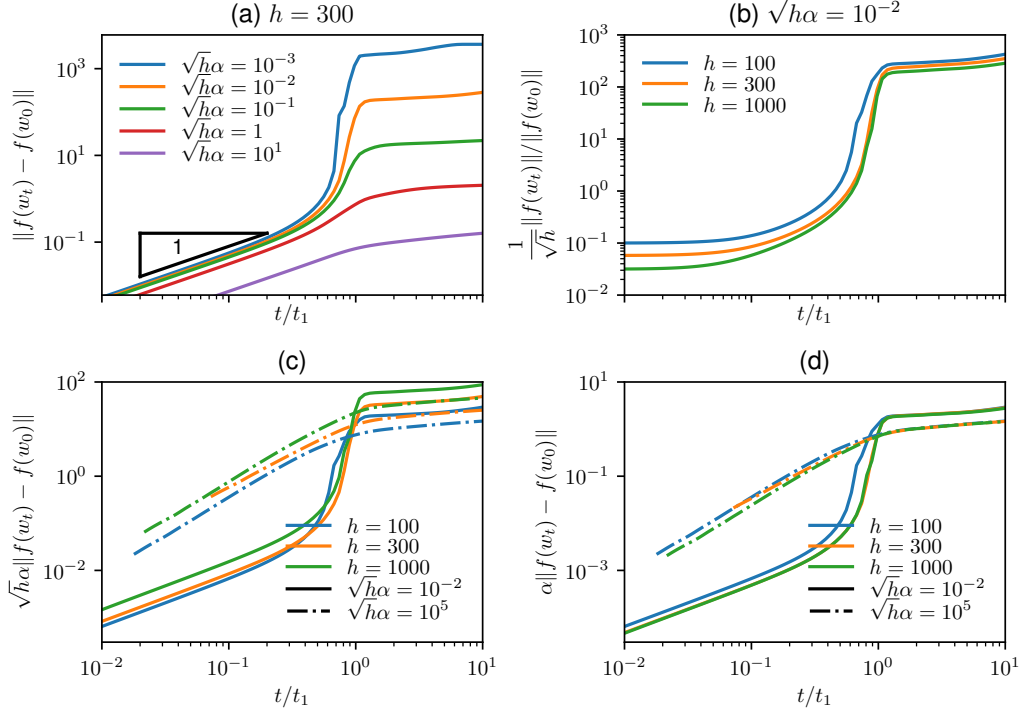


Figure 10: Different measures of the network norm v.s. t/t_1 for (a) a fixed width h and various α , (b,c,d) a fixed value of $\sqrt{h}\alpha$ and various h . Here t_1 is the time at which the loss reduced by half. The network used here has $L = 2$ hidden layers and uses a *Softplus* activation function. Each curve is averaged along the y axis for 10 realizations.

D Preactivation evolution

Fig. 11 shows the amplitude of $\dot{\tilde{z}}$ at initialization. We measured it using finite-difference method by applying a single gradient descent step.

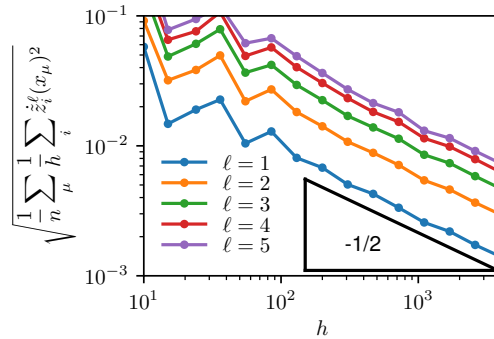


Figure 11: $\dot{\tilde{z}}$ at $t = 0$ v.s. h for different layers. Each measure is averaged over 5 networks. The network used here has $L = 5$ hidden layers and uses a *Softplus* activation function.

E Shallow network

In order to verify the depth dependence of our heuristic predictions about the powerlaw in α of the quantities $\|\Theta - \Theta_0\|$ and $\|w - w_0\|$, we reran the experiment with 2 hidden layers ($L = 2$) with the fully-connected network and *Softplus*. In Table 2 we summarize the exponent found numerically, they are compatible the our predictions.

Observable	$L = 5$	$L = 2$	Prediction
$\ \Theta - \Theta_0\ $	1.7 (1.66)	1.25 (1.33)	$\frac{2}{1+1/L}$
$\ w - w_0\ $	0.23 (0.166)	0.35 (0.333)	$\frac{1}{1+L}$

Table 2: Powerlaw dependence in α , measure and prediction (in parenthesis) of the exponent a where $O \sim \alpha^{-a}$ for $\alpha \ll 1$

F ReLU activation function

Fig. 12 shows the evolution of the kernel as a function of $\sqrt{h}\alpha$ for a network with *ReLU* activation function. Differently from the *Softplus* case (see Fig. 5 (a)), here we observe the existence of three regimes, each characterized by a different power law. The intermediate regime with slope $-1/2$ is not present for *Softplus*, and it is compatible with the following explanation. The *ReLU* function $x \mapsto \max(0, x)$ is non differentiable in $x = 0$. It implies that $w \mapsto f(w)$ is not differentiable. For a finite dataset, $w \mapsto \{f(w, x_\mu)\}_\mu$ is differentiable only on small patches. As we can see in Fig. 12 for large enough α , w evolution is so small that f remains in a differentiable patch and we get the predicted result of slope -1 . But for intermediate values of α , the network change patches a number of times proportional to α^{-1} and assuming that each changes in the kernel induced by these changes of patch are not correlated, their sum scales with $\alpha^{-1/2}$.

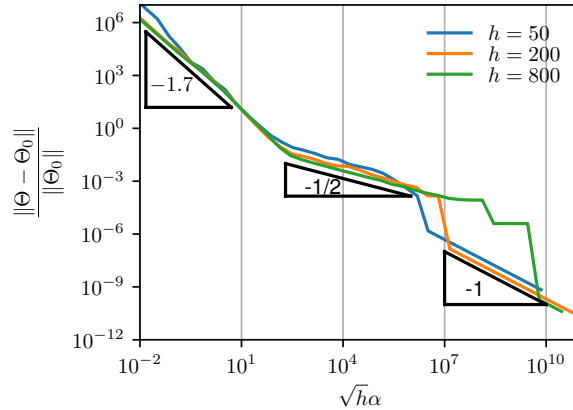


Figure 12: $\frac{\|\Theta - \Theta_0\|}{\|\Theta_0\|}$ v.s. $\sqrt{h}\alpha$ for different heights. Each measure is averaged over 3 networks. The network used here has $L = 5$ hidden layers and uses a *ReLU* activation function.

G Gradient flow and momentum dynamics verification

As we can see in Fig. 13(a), the constraint we put on the relative difference of gradients for the dynamics ensure that the relative difference of the output is smaller than 10^{-3} when the constraint is divided by 100. Fig. 13(b) shows that the momentum we set is relatively small in the sense that dividing it by 10^4 almost does not affect the output. We can see that the effect of momentum is larger for small $\sqrt{h}\alpha$.

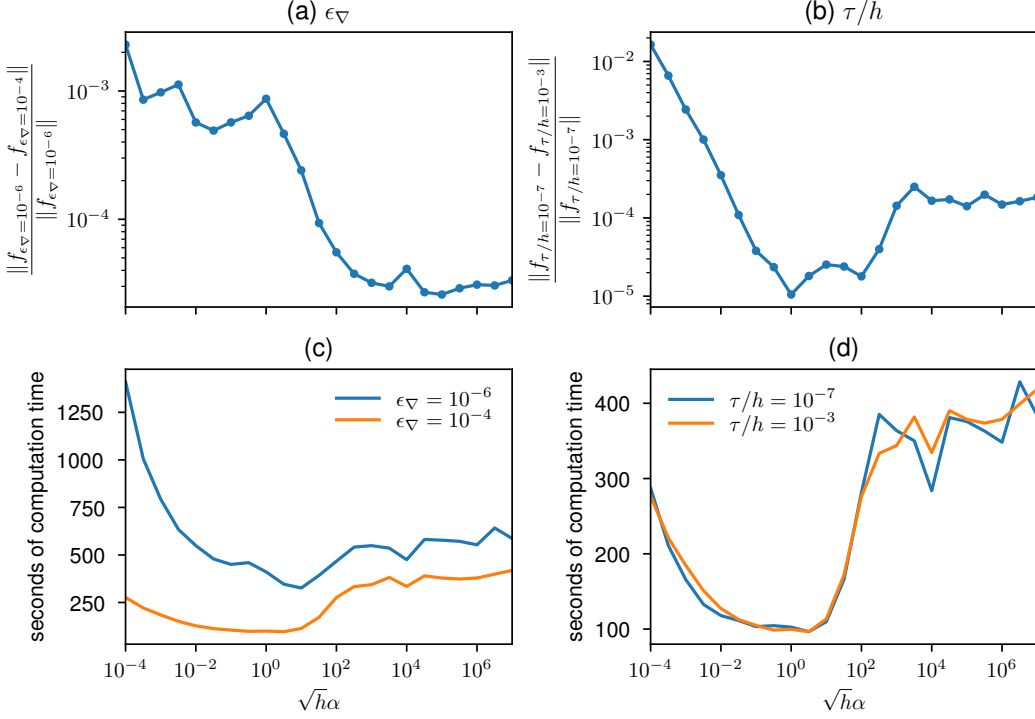


Figure 13: (a) Relative difference of the output for two different values of ϵ_{∇} v.s. $\sqrt{h}\alpha$. (b) Relative difference of the output for two different values of τ/h v.s. $\sqrt{h}\alpha$. (c) Computation time v.s. $\sqrt{h}\alpha$, for two different values of ϵ_{∇} . (d) Computation time v.s. $\sqrt{h}\alpha$, for two different values of τ/h .

H Variance and the size of the dataset in the lazy-training regime

In Fig. 14 the variance is shown as a function of the width, for different sizes of dataset n . (i) We see the variance reaching the asymptotic behavior of h^{-1} when n is small enough. (ii) The data also suggest that the variance grows with the size of the trainset like \sqrt{n} .

$$\text{Var} f(w, x) = \left\langle [f(w_i, x_\mu) - \bar{f}(x_\mu)]^2 \right\rangle_{\substack{\mu \in \text{test} \\ i \in \text{ensemble}}} . \quad (34)$$

I $f - f_0$ versus f

Fig. 15 shows the difference between the model $F(w, x) = \alpha f(w, x)$ and $F(w, x) = \alpha(f(w, x) - f(w_0, x))$. Notice that removing the value of the output function at initialization drastically improves the performance of the network for large values of α . The generalization error is the same for small α .

J Effect of biases

In Fig. 16 we test the helpfulness of introducing biases in hidden layers, by comparing the test error and the variance of the output function in networks that have or have no biases. It turns out that biases are negligible in the present setting. The setup is described in Section 2. A possible reason to use biases would be that ReLU networks without biases are homogeneous functions. This mean that two data x_μ, x_ν that are *aligned*, in the sense that $x_\mu = |\lambda|x_\nu$, cannot have different labels. This problem can often be neglected for two reasons: first, in practice the datasets are normalized, so that two points are aligned only if they are identical; second, the pictures in some datasets typically have

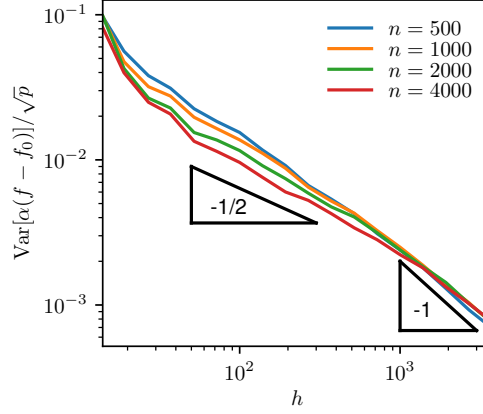


Figure 14: Variance of the output in the lazy-training regime ($\sqrt{h}\alpha = 10^6$) v.s. the network's width h for different size of trainset n . We believe that eventually all the curves asymptote with a slope -1. This asymptote is reached earlier for smaller n .

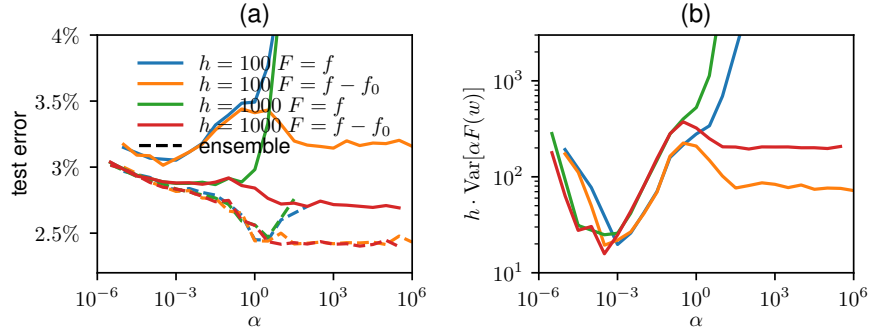


Figure 15: Comparison of the model $f(w) - f(w_0)$ with $f(w)$. The setup is described in Section 2. (a) Test error (single shot and ensemble average) v.s. α for a network of two widths and the two models. (averaged over 10 initializations) (b) The network's width time the variance of the output v.s. α . (averaged over 10 initializations)

constant pixels. For instance, in MNIST the top-left pixel in every picture is black. Constant pixels behave effectively as a bias in any hidden neuron.

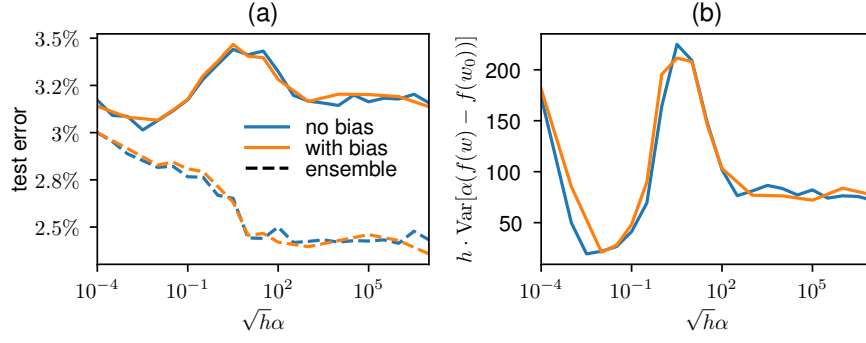


Figure 16: Same as Fig. 3 but with biases. (a) Test error (single shot and ensemble average) v.s. $\sqrt{h\alpha}$ for a network of width $h = 100$, averages are over 20 initializations. (d) We plot the width times the variance of the output function v.s. $\sqrt{h\alpha}$, averaged over 10 initializations.